Pressure-induced Superionicity of H^- in Hypervalent Sodium Silicon Hydrides

Tianxiao Liang[1], Zihan Zhang[1], Hongyu Yu[1], Tian Cui[2,1,], Xiaolei Feng[3,4,*], Chris J. Pickard[5,6], Defang Duan[1,*], and Simon A. T. Redfern[7]*

[1] State Key Laboratory of Superhard Materials, College of Physics, Jilin University, Changchun 130012, China

[2] Institute of High Pressure Physics, School of Physical Science and Technology, Ningbo University, Ningbo 315211, China

[3] Institute for Disaster Management and Reconstruction, Sichuan University - the Hong Kong Polytechnic University, Chengdu 610207 China

[4] Department of Earth Sciences, University of Cambridge, Downing Street, Cambridge CB2 3EQ, United Kingdom

[5] Department of Materials Science and Metallurgy, University of Cambridge, 27 Charles Babbage Road, Cambridge CB3 0FS, United Kingdom

[6] Advanced Institute for Materials Research, Tohoku University 2-1-1 Katahira, Aoba, Sendai 980-8577, Japan

[7] Asian School of the Environment, Nanyang Technological University, Singapore 639798

ABSTRACT. Superionic states simultaneously exhibit properties of a fluid and a solid. Proton (H^+) superionicity in ice, H_3O, He-H_2O and He-NH_3 compounds is well-studied. However, hydride (H^-) superionicity in H-rich compounds is rare, being associated with instability and strongly reducing conditions. Silicon, sodium, and hydrogen are abundant elements in many astrophysical bodies. Here, we use first principles calculations to show that, at high pressure, Na, Si, and H can form several hypervalent compounds. A previously unreported superionic state of Na_2SiH_6 results from unconstrained H^- in the hypervalent $[SiH_6]^{2-}$ unit. Na_2SiH_6 is dynamically stable at low pressure (3 GPa), becoming superionic at 5 GPa, and re-entering solid/fluid states at about 25 GPa. Our observation of H^- transport opens up a new field of H^- conductors. It also has implications for the formation of conducting layers at depth in exotic carbon exo-planets, potentially enhancing the habitability of such planets.

TOC GRAPHICS

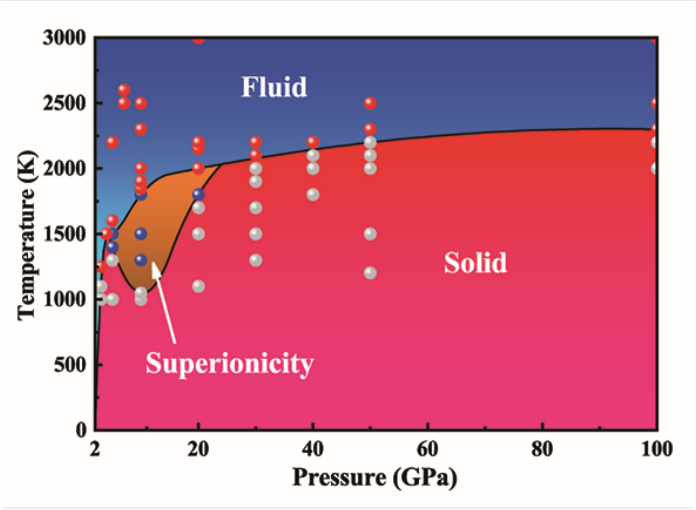

Superionicity in hydrogen-bearing solids. Several recent results suggest the possible existence of superionic conducting solid ices in the interiors of gas giants such as Uranus and Neptune, with superionic water and ammonia ices and liquids first identified as thermodynamically stable under the appropriate conditions of pressure and temperature [1-3]. More recently Liu *et al.* [1, 2] predicted a number of superionic helium compounds in the He-H_2O [1], He-NH_3 [2], and He-CH_4 [3] systems to be stable at similar high pressures and temperatures. It was demonstrated that He and protons (H^+) can freely diffuse in the $I4_1md$ or $Fd\bar{3}m$ lattices of crystalline He_2H_2O, resulting in two different types of superionic phases. Independently, Shi et al. also predicted $(NH_3)_2He$ has a superionic phase at 2000 K and 100 GPa [4]. Superionicity associated with unconstrained H^- ions has been reported to emerge in NH_3-H_2 mixtures [5]. Experimental electrical conductivity measurements [6, 7], Raman spectroscopy [8] and X-ray diffraction [9] of ice under compression all support the existence of superionic states. Superionicity has also been reported in FeO_2H by Hou et al [10]. Additional structural prediction studies by Huang et al. also proposed the existence of superionic H_3O under the conditions of the deep interior of Uranus or Neptune [11]. Thus, it becomes apparent that, under the appropriate conditions of temperature and pressure, H^+ can also freely diffuse in the crystalline host lattices of a number of He-NH_3 compounds as well as H_2O ice and H_3O. It is, therefore, believed that planetary deep interior environments corresponding to those of gas giants may host superionic materials [12-15].

Aside from their potential importance in the interiors of gas giants, superionic materials have attracted considerable interest in wide range of applications. In particular, fast ion conductors and solid electrolytes have, in recent years, been relevant to the developments of lithium-ion batteries [16-18] and other applications of Li-based superionic conductors [19, 20]. While H^+ is common in the nature, unconstrained hydride ions (H^-) are believed to be unstable and only emerge in

hydrogen-storage alloys and electrolytes in all-solid-state batteries, because of strong reducing conditions. As an important reducing agent of all-solid-state batteries, the mechanism describing H^- transport in many H^- conducting materials has been well studied [21-23].

Silicon is the eighth most abundant element in the universe, the third most abundant in the bulk Earth, and the second most abundant (28.2%) in the crust. Sodium is the sixth most abundant (2.36%) element in Earth's crust, where it is the most abundant alkali metal. Of course, hydrogen is the most abundant element in the universe. The possibility of silanes forming as precursors to early life has been suggested by a number of authors, reviewed in Petkowski et al. [24] recently. Indeed, it may be the case that alkali silanes could form a component of the building blocks of planets forming under extremely reducing conditions, not least carbon planets. The behavior of silanes under high pressure has generated some interest in view of their potential as a route towards the formation of metallic hydrogen [25-27], but the properties of alkali-silicon-hydrides has also potential relevance to the formation of exotic exoplanets: sodium hydrides have been suggested in exoplanetary atmospheres [28]. Visscher et al. [29] suggested that, while SiO will be prevalent in the atmospheres of exoplanets and brown dwarf stars at low pressures, on increasing pressure silane should become the most abundant silicon species. Furthermore, Yurchenko et al. [30] demonstrate that species such as SiH may be present following reaction with SiO. Alkali silicon hydrides may well form in such high-pressure environments, and their behavior and properties at the conditions of exoplanetary interiors is of particular importance.

Hypervalences are well established in chemistry, in which central atoms attain an environment of valence electrons that exceeds eight through their coordination with ligands [31]. The Lewis-Langmuir theory of valence attributed the stability of molecules to their ability to place their valence electrons, when appropriately paired off as chemical bonds, into stable octets. In 2012,

Puhakainen et al. showed that $Fm\bar{3}m$-K_2SiH_6 with octahedral-structured $[SiH_6]^{2-}$ anions could be synthesized by potassium hydride (KH), potassium silicide (KSi), silicon, and hydrogen via reactions KH + Si + H_2 or KSi + H_2 at pressures above 4 GPa and temperatures between 450-650 °C [32]. More recently, Liang et al. [33] and Zhang et al. [34] proposed the existence of several different types of Li-Si-H compounds, including layer-type $[SiH_5]^-$ in $LiSiH_5$, and tricapped triangular prismatic $[SiH_6]^{2-}$ in Li_2SiH_6, and $LiSi_2H_9$ and $LiSiH_8$ superconductors.

Here we extend this study of alkali silicon hydrides by an exploration of the sodium system and uncover several ternary Na-Si-H phases that exist with unusual structures and properties at high pressure. Remarkably, we find a novel H^- conducting material, $P\bar{3}m1$ $-Na_2SiH_6$, with hypervalent H-rich structure, which displays unexpected superionicity of H^- in its covalent framework and shows a quite different mechanism from both hydride ions conductors in all-solid-state batteries and proton superionic conductors. In addition, we propose the probable phase diagram of Na_2SiH_6 and suggest potential conditions for exoplanetary paragenesis.

Computational methods. Structure searches in the system Na-Si-H were performed using ab initio calculations as implemented in the AIRSS (Ab Initio Random Structure Searching) code [35, 36] combined with CASTEP (Cambridge Sequential Total Energy Package) [37]. Full variable-composition predictions were firstly performed within 50,000 structures at pressures of 10 GPa, 50 GPa, 100 GPa, and 200 GPa. Then, fixed composition predictions were employed to further search structures for stable compounds. The VASP (Vienna ab initio simulation packages) code [38] was used to optimize crystal structures and calculate the electronic properties, where the Perdew–Burke–Ernzerhof [39] implementation of the generalized gradient approximation was performed. The electron-ion interaction was described using projector-augmented-wave potentials [40] with the $1s^1$, $2s^2 2p^6 3s^1$ and $2s^2 2p^6 3s^2 3p^2$ configurations treated as valence electrons for

H, Na and Si, respectively. The kinetic cutoff energy of 800 eV, and Monkhorst-Pack **k** meshes with grid spacing of $2\pi \times 0.03\mathring{A}^{-1}$ were adopted to ensure the enthalpy converged to less than 1 meV/atom. The phonon calculations were implemented in the PHONOPY code [41]. The crystalline orbital Hamilton populations (COHPs) were calculated as implemented in the LOBSTER [42] package, to investigate the Si-H bonding characteristics. Bader charge analysis [43] was used to determine charge transfer, and the electron localization function (ELF) [44] was used to describe and visualize chemical bonds in molecules and solids.

To explore the dynamical properties, we performed extensive ab initio molecular dynamics (AIMD) simulations based on the Born-Oppenheimer approximation implemented in VASP within the pressure range 3 to 200 GPa and set the temperature range 1,000-3,000 K. AIMD simulation were performed in $3\times3\times3$ supercells (243 atoms) for $P\bar{3}m1$ $-Na_2SiH_6$, with Γ-centered k point. We also used $4\times4\times4$ supercells (576 atoms), $5\times5\times5$ supercells (with 1125 atoms) and $2\times2\times2$ k mesh to test the convergence. We adopted the canonical *NVT* ensemble, lasting for 12 ps with a time step of 1 fs, and we allowed 2 ps for thermalization and then extracted data from the last 10 ps. Some simulations were extended to 30 ps to check stability. MDAnalysis codes [45, 46] were used to postprocess the data.

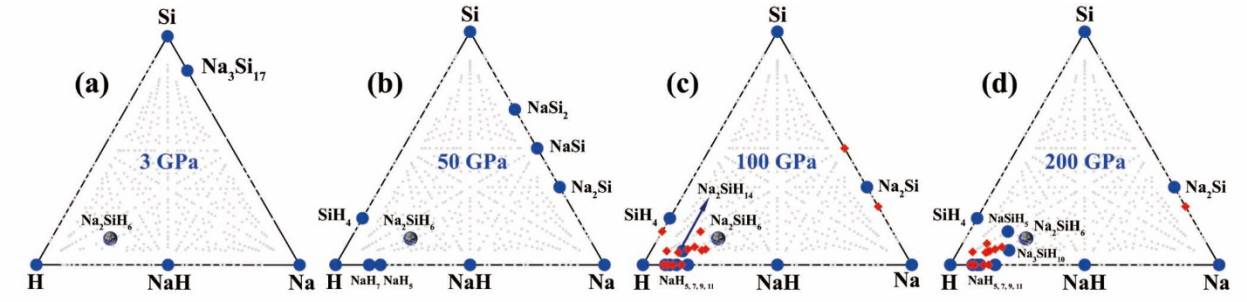

Figure 1. The Na-Si-H ternary phase diagram as a function of pressure. Large purple circles represent compounds located on the convex hulls, and Na_2SiH_6 located on the convex hulls is in

particular picked out by the small Earth symbol. Small red diamonds represent structures which are located above the convex hulls.

Stability, structure and properties of Na-Si-H compounds. We have performed an extensive exploration of the high-pressure phase stabilities of phases within the Na-Si-H system using the random structure searching method implemented in the AIRSS code. This has led to the discovery of four stable ternary stoichiometries, $NaSiH_5$, Na_2SiH_6, Na_3SiH_{10}, and Na_2SiH_{14}, as shown in Figure 1. At 3 GPa, Na_2SiH_6 is the only ternary structure located on the convex hull. As pressure increases, more and more ternary stoichiometries become thermodynamically stable. These include Na_2SiH_6 and Na_2SiH_{14} located on the convex hull at 100 GPa. On further pressure increases, $NaSiH_5$, Na_2SiH_6, and Na_3SiH_{10} all appear on the convex hull at 200 GPa. Furthermore, Na_2SiH_8, Na_2SiH_{10}, Na_2SiH_{12}, and Na_2SiH_{16} are less than 2 meV/atom above the convex hull at 200 GPa, and are dynamically stable. We note that Na_2SiH_6 is the only phase stable across the entire pressure range of 3 to 200 GPa.

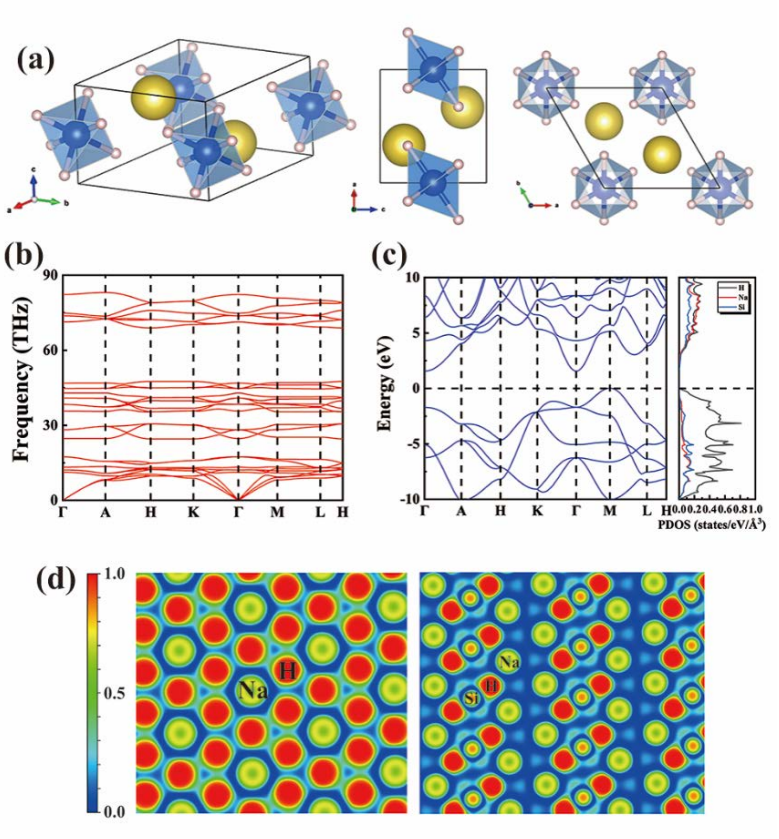

Figure 2. Crystal structure and properties of Na_2SiH_6. (a) Crystal structure projected in different directions. (b) Phonon dispersion relations at 100 GPa. (c) Electronic band structures and projected density of states at 100 GPa. (d) ELF calculation in (0, 0, 1) and (2, -1, 0) sections**.**

Na_2SiH_6 adopts a structure with trigonal $P\bar{3}m1$ symmetry, in which each Si is bonded to six H forming octahedra $[SiH_6]^{2-}$ groups (Figure 2(a)), with no phase transition observed up to 200 GPa. The absence of imaginary frequencies in the phonon spectra in Figure 2(b) indicates that $P\bar{3}m1-Na_2SiH_6$ is dynamically stable. As shown in Figure S1 in the supplementary material (SM), Na_3SiH_{10} and $Na_2SiH_{6+\delta}$ (δ = 2,4,6,8,10) also form structures based on octahedra $[SiH_6]^{2-}$ anions, and there are many H_2 units extended into different directions in their cells reducing their symmetries to $P\bar{1}$. At 200 GPa, we found a structure of $NaSiH_5$ which adopts the same layer-typed phase as $LiSiH_5$ seen in Liang *et al.*'s [33] work (see Figure S1(a) and Figure S2 in the SM), and

another different linear-type structure also composed of $[SiH_6]^{2-}$ anions forming in space group *Imm*2-Na_2SiH_{12} (see Figure S3 in the SM). Predicted structural parameters of these ternary compounds are listed in Table S1, and are listed in Figure S4-S11 in the SM.

We examined the electronic properties of these predicted Na-Si-H compounds, and Bader charge analysis reveals a charge transfer from Na/Si to H (Table S2 in the SM), suggesting that both Na and Si are electron donors and provide electrons to H. Na constantly loses approximate 0.75-0.81 e^- per atom and Si loses approximate 2.6-3.0 e^- per atom in the stable phases. The electronic band structure calculations and the projected density of states, given in Figure 2(c), demonstrate that Na_2SiH_6 is an insulator with a wide band gap. Almost all of Na-Si-H compounds are semiconductors or insulators with band gaps greater than 1 eV, as shown in Figure S12-19 in the SM. Figure 2(d) shows the articulated skeleton constructed by octahedral $[SiH_6]^{2-}$ molecular anions. To investigate the Si-H bonding characteristics, we calculated the COHP of Si-H bonds in Na_2SiH_6 depicted in Fig. S20 in the SM. The integrated COHP values of Si-H bond is -4.05 at 10 GPa and -4.23 at 20 GPa indicating that bonding between Si and H is covalent. In addition, the Si-H distance is 1.583 Å at 10 GPa (Table S3) which is larger than other Na-Si-H compounds.

Superionicity of Na_2SiH_6. We have also studied the dynamical properties of Na_2SiH_6, which is stable over a relatively large and continuous pressure range. We performed extensive *ab initio* molecular dynamics (AIMD) simulations within the pressure range 3-200 GPa and temperature range 1,000-3,000 K. Atomic diffusion coefficients (*D*) of H, Si, and Na were calculated from the mean-square displacements (MSDs) as shown in Figure 3(a)-(c). Surprisingly, we found a region of superionicity with extraordinary diffusive H. This superionic phase can be classified as one of three phases in terms of the diffusion coefficient (*D*) of the H atoms: the solid phase ($D_{\mathrm{H}} = D_{\mathrm{Na}} = D_{\mathrm{Si}} = 0$), the fluid phase ($D_{\mathrm{H}} > 0$, $D_{\mathrm{Na}} > 0$, and $D_{\mathrm{Si}} > 0$), and the superionic (SI) phase ($D_{\mathrm{H}} > 0$

but $D_{Na} = D_{Si} = 0$), and Si-H atomic trajectories of (1, 0, 0) Si-H layers are correspondingly provided in Figure 3(d)-(f).

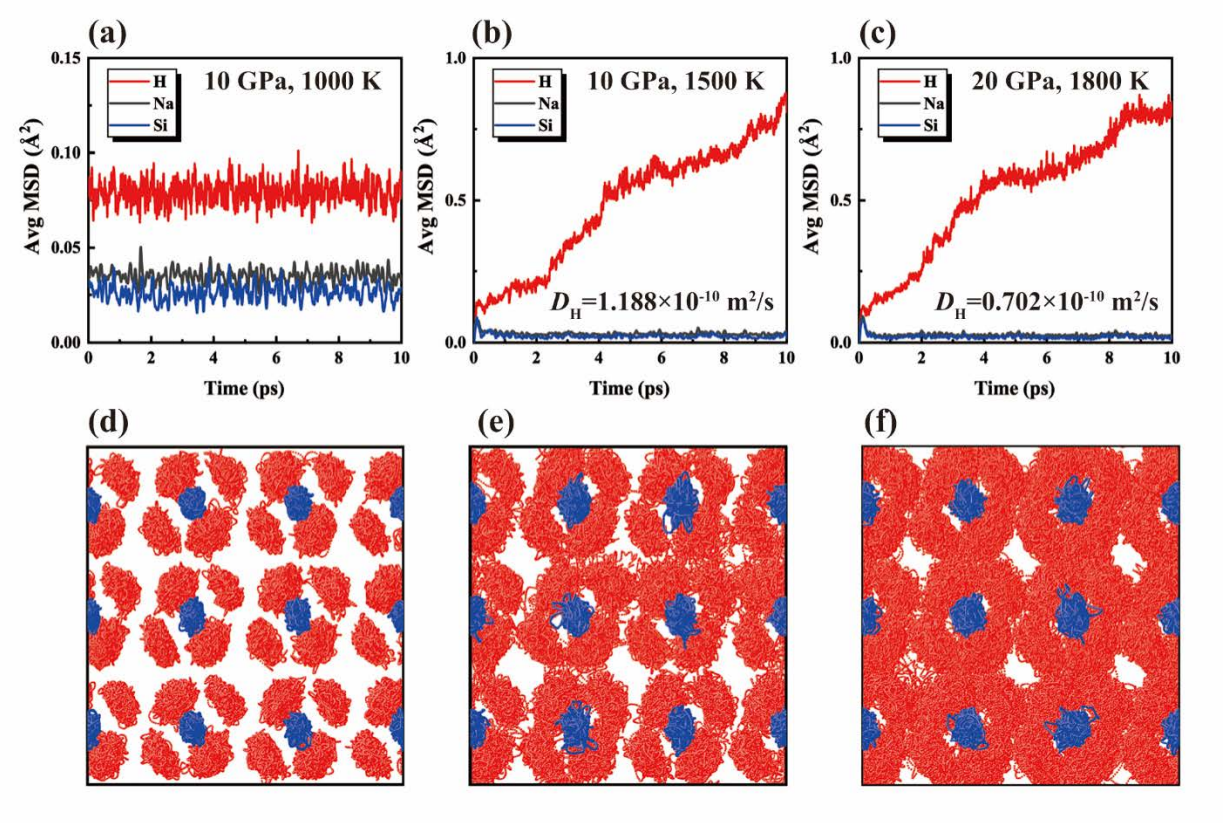

Figure 3. Dynamical behaviors of H (red) and Na (grey) atoms compared to Si atoms (blue) in the Na-Si-H compounds under high pressure and temperature. MSD calculated from the AIMD simulations for Na_2SiH_6 compounds in the solid and superionic states. (a)-(c) are the averaged mean-squared displacements (Avg MSD) under different pressures and temperatures. We obtain the diffusion coefficients D_H from the slopes of MSD curves. (d)-(f) are the representations of atomic trajectories in one supercell from the simulations for three distinct phases: (d) the solid phase (10 GPa and 1,000 K), (e) the superionic phase (10 GPa and 1,500 K), (f) the superionic phase (20 GPa and 1,800 K). Only (1, 0, 0) Si-H layers are plotted in (d)-(f), and the Si and H atoms are dividedly plotted in blue and red.

At 10 GPa and 1,000 K, Na_2SiH_6 is a solid phase with all atoms vibrating around their equilibrium positions in the crystal structure and diffusion coefficients of $D_H = D_{Na} = D_{Si} = 0$, as shown in Figure 3(a). In the same structure, as temperature increases above 1,500 K, the H atoms appear diffusively mobile with $D_H = 1.188 \times 10^{-10}$, while the Na and Si atoms still keep vibrating around their mean lattice positions. This suggests that the solid Na_2SiH_6 transforms to the superionic conducting state at this condition. Finally, upon increasing the temperature all the way up to 1,800 K, all the atoms diffuse freely indicating melting of Na_2SiH_6 (not shown here). The superionicity of Na_2SiH_6 is first observed at about 5 GPa and 1400 K. At 10 GPa, it tends to be an insulating solid until the temperature reaches to 1,050 K, at which point the material transforms to a superionic conductor. When the temperature increases above 1,800 K, Na_2SiH_6 appears to become fluid. At 20 GPa, $P\bar{3}m1$ $-Na_2SiH_6$ appears to be an insulating solid up to 1,800 K, then becomes superionic, becoming fully fluid above 2,000 K. High pressure inhibits the diffusion of H atoms but high temperature enhances the diffusion of H atoms (Table S4 in the SM), which is reflected in the values of D_H in Figure 3. Calculations on larger supercells with $4 \times 4 \times 4$ supercells (576 atoms) and $5 \times 5 \times 5$ supercells (1125 atoms) were also performed, and we obtained similar diffusion coefficients of D_H, D_{Na} and D_{Si}, compared to $3 \times 3 \times 3$ supercells.

We note that D_H of H atoms in superionic $P\bar{3}m1$ $-Na_2SiH_6$ is of the order of 10^{-10}-10^{-11} m^2/s, which is lower than H atomic diffusion in Ni-H at ambient pressure and 1000 K (estimated as 10^{-7}-10^{-8} m^2/s) [47], and also lower than H diffusion in He-H_2O/He-NH_3 compounds under ice giant planet conditions (estimated as 10^{-8}-10^{-10} m^2/s) [1, 2]. It is common practice to express the diffusion coefficient in the form:

$$\ln\left(\frac{D}{D_0}\right) = -\frac{Q}{RT} \quad (1)$$

where Q is the height of the activation barrier, D_0 is a pre-factor which is often assumed to be independent of the temperature T, and R is the gas constant. At 10 GPa, a linear fit between 1500 and 1700 K of the computed data for D_H of H atoms in superionic $P\bar{3}m1$ $-Na_2SiH_6$ gives Q = 39.50 kJ/mol (0.42 eV), and D_0 = 1.201×10^{-10} m^2/s. The activation barrier for H diffusion in superionic $P\bar{3}m1$ $-Na_2SiH_6$ is a little higher than that of about 0.4 eV suggested for hydrogen-oxygen fuel cells [21, 22]. As shown in Figure 3(e) and (f) for atomic trajectories in the superionic phase, H atoms move freely around adjacent Si atoms.

The diffusion velocity of H^- in Na_2SiH_6 is much slower than both H^- conductors in all-solid-state batteries and superionicity of H^+ such as H_2OHe_2. In traditional hydride ionic conductors, H^- is always associated with vacancies or high symmetry sites and does not support the structure of parent materials, so the activation barrier of H^- transport between vacancies is faster than that in the strong bonding structures such as Na_2SiH_6 presented here. Comparing the diffusivity with H^+ transport seen in materials such as that in H_2OHe_2, H^- occupies a larger volume, which explains the lower diffusion velocity of H^- compared to that of H^+.

We further explored the dynamic properties of the other stable Na-Si-H compounds identified by our structure searches. In particular, we have calculated averaged mean-squared displacements (MSD) of ternary stoichiometries $NaSiH_5$, Na_3SiH_{10}, and Na_2SiH_{14} at their stable pressures and 2000 K. Unlike Na_2SiH_6, our results do not indicate superionic behavior in any of these phases.

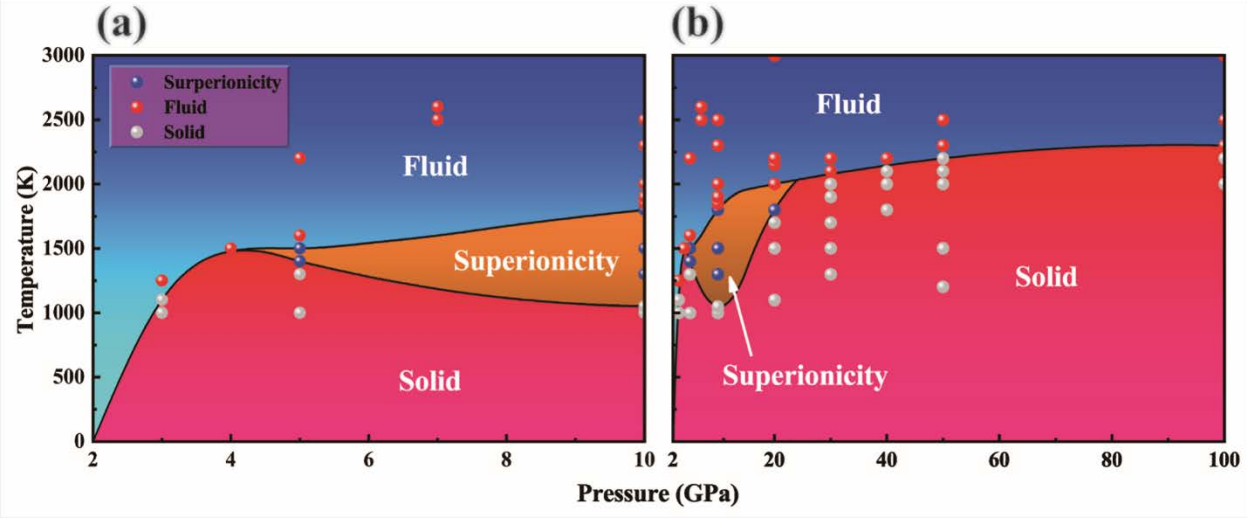

Figure 4. Proposed phase diagram of Na_2SiH_6 at high pressure and temperature obtained from structure searches and AIMD simulations. (a) Detailed phase diagram from 2-10 GPa. (b) Total phase diagram from 2-100 GPa. Different colored spheres are used to mark the simulations. Na_2SiH_6 shows three different phases as temperature and pressure changing, which are liquid phase, solid phase, and superionic phase.

Pressure-temperature phase diagram of Na_2SiH_6. Inspired by the temperature-induced features in Na_2SiH_6 discussed above, we expanded the pressure range studied to explore the superionic region from ambient pressure up to about 100 GPa with pressure steps of 10 GPa in Figure 4(b), and calculated the region from ambient pressure up to 10 GPa in detail with pressure steps of 1 GPa in Figure 4(a). Each of colored spheres in Figure 4(a)-(b) corresponds to an independent simulation. As shown in Figure 4(a)-(b), two different melting curves divide the phase diagram of Na_2SiH_6 into three regions: solid, superionic and fluid. The thermal fluctuations of Na_2SiH_6 increase rapidly across the low-pressure range. In the superionic state, the thermal fluctuations increase more gradually above 20 GPa. Finally, superionicity is inhibited with increasing pressure and finally disappears at higher pressures. The melting curve dividing solid and liquid flattens off above 30 GPa. The conditions seen here represent those typical of modest depths (of the order of

100s of km) in planetary interiors and suggest the potential prevalence of ionic conductivity in carbon exo-planets. Such conductivity will typically induce magnetic fields, with subsequent implications for the formation and retention of planetary atmospheres and habitability.

The law of equipartition of energy implies that, at equilibrium, the energy should be equally distributed among the degrees of freedom. Thus, lighter atoms with the same kinetic energy should move faster than heavier atoms in non-interacting systems. Within our Na-Si-H compounds, H atoms from $[SiH_6]^{2-}$ ions show greater mobility. Combining the Bader analysis results (Table S2), the radial distribution functions (RDF) (Fig S22), and dynamic behaviors of atoms of Na_2SiH_6 (Table S4 in the SM), we find that the H^- in the $[SiH_6]^{2-}$ ions move fastest and play an important role in charge transport, which is contrasts with observations of the behavior of H^+ in earlier work [1, 2, 11]. The temperature and pressure that we predict would be required for synthesis of superionic state of Na_2SiH_6 are much lower and more accessible than those predicted for the synthesis of superionic water, H_3O, or He-H_2O/He-NH_3 compounds, which suggests it may be possible to observe this phenomenon by measuring the electrical conductivity of H^- in $[SiH_6]^{2-}$ [6, 7].

In summary, our crystal structure searches with AIRSS and first-principles calculations have identified several stable or meta-stable hypervalent structures, which are dynamically stable at high pressure conditions. Several different types of hypervalent ions were discovered with layer-typed $[SiH_5]^-$ and linear $[SiH_6]^{2-}$. For $P\bar{3}m1$ $-Na_2SiH_6$, we find a H^- superionic conductor at high pressure and temperature and suggest a novel mechanism of hydride ion transport in hypervalent structures. At relatively low pressures of 3 GPa, the superionic region exists and is increasingly inhibited by increasing pressure up to above 10 GPa, where it finally disappears. Superionic states of Na_2SiH_6 appear at much lower pressure and temperature conditions than those predicted for hot

ice or other H^+ superionic compounds, which suggests this behavior may be more easily accessed in future experiments. Our findings propose a class of hydride ion conductors with hypervalent structures that have not previously been recognized, furthering our understanding of superionicity associated with hydride ions. We note that the conditions at which we see superionic behavior correspond to those of modest depths in planetary interiors. Since hydrides, such as Na_2SiH_6, are likely stable in the planetary interiors of carbon exo-planets, our results indicate that such bodies may be able to sustain long-term magnetic fields, increasing their potential for the development of planetary atmospheres and exotic life forms.

AUTHOR INFORMATION

Corresponding Authors

Tian Cui - *Ningbo University, Ningbo, China; Jilin University, Changchun 130012, China;* orcid.org/0000-0002-9664-848X; Email: cuitian@nbu.eu.cn

Xiaolei Feng - *Sichuan University, Chengdu, China; University of Cambridge, United Kingdom;* orcid.org/0000-0003-4410-4576*;* Email: xf232@cam.ac.uk

Defang Duan - *Jilin University, Changchun, China;* orcid.org/0000-0002-6878-1830; Email: duandf@jlu.edu.cn

Other Authors

Tianxiao Liang - *Jilin University, Changchun, China;* orcid.org/0000-0001-9932-2314; Email: liangtx18@mails.jlu.edu.cn

Zihan Zhang - *Jilin University, Changchun, China;* orcid.org/0000-0003-3374-9539; Email: zhz19@mails.jlu.edu.cn

Hongyu Yu - *Jilin University, Changchun, China;* Email: yuhongyu@jlu.edu.cn

Chris J. Pickard - *University of Cambridge, United Kingdom; Tohoku University, Japan;* orcid.org/0000-0002-9684-5432; Email: cjp20@cam.ac.uk

Simon A. T. Redfern - *Nanyang Technological University, Singapore;* orcid.org/0000-0001-9513-0147; Email: simon.redfern@ntu.edu.sg

Author Contributions

T.C. and D.D. designed the project. T.L., Z.Z. and H.Y. performed the calculations. T.L., Z.Z., X.F., C.J.P., D.D. and S.A.T.R. analyzed the data. T.L., X.F., C.J.P., D.D. and S.A.T.R. wrote the manuscript. All authors discussed the results and commented on the manuscript.

Notes

The authors declare no competing financial interests.

ACKNOWLEDGMENTS

This work was supported by the National Key R&D Program of China (No. 2018YFA0305900), National Natural Science Foundation of China (Nos. 11674122, 51632002 and 52072188). CJP acknowledges financial support from the Engineering and Physical Sciences Research Council [Grant EP/P022596/1]. Parts of calculations were performed in the High Performance Computing Center (HPCC) of Jilin University and TianHe-1(A) at the National Supercomputer Center in Tianjin.

REFERENCES

1. Liu, C.; Gao, H.; Wang, Y.; Needs, R. J.; Pickard, C. J.; Sun, J.; Wang, H.; Xing, D. Multiple superionic states in helium-water compounds. Nat. Phys. 2019. **15**(10) 1065-1070.
2. Liu, C.; Gao, H.; Hermann, A.; Wang, Y.; Miao, M.; Pickard, C. J.; Needs, R. J.; Wang, H.; Xing, D.; Sun, J. Plastic and superionic helium ammonia compounds under high pressure and high temperature. Phys. Rev. X 2020. **10**(2) 021007.
3. Gao, H.; Liu, C.; Hermann, A.; Needs, R. J.; Pickard, C. J.; Wang, H.; Xing, D.; Sun, J. Coexistence of plastic and partially diffusive phases in a helium-methane compound. Natl. Sci. Rev. 2020. **7**(10) 1540-1547.
4. Shi, J.; Cui, W.; Hao, J.; Xu, M.; Wang, X.; Li, Y. Formation of ammonia-helium compounds at high pressure. Nat. Commun. 2020. **11**(1) 1-7.
5. Song, X.; Yin, K.; Wang, Y.; Hermann, A.; Liu, H.; Lv, J.; Li, Q.; Chen, C.; Ma, Y. Exotic hydrogen bonding in compressed ammonia hydrides. J. Phys. Chem. Lett. 2019. **10**(11) 2761-2766.
6. Chau, R.; Mitchell, A. C.; Minich, R. W.; Nellis, W. J. Electrical conductivity of water compressed dynamically to pressures of 70-180 GPa (0.7-1.8 Mbar). J. Phys. Chem. 2001. **114**(3) 1361-1365.
7. Yakushev, V. V.; Postnov, V. I.; Fortov, V. E.; Yakysheva, T. I. Electrical conductivity of water during quasi-isentropic compression to 130 GPa. J. Exp. Theor. Phys. 2000. **90**(4) 617-622.
8. Goncharov, A. F.; Goldman, N.; Fried, L. E.; Crowhurst, J. C.; Kuo, I. W.; Mundy, C. J.; Zaug, J. M. Dynamic ionization of water under extreme conditions. Phys. Rev. Lett. 2005. **94**(12) 125508.
9. Millot, M.; Coppari, F.; Rygg, J. R.; Barrios, A. C.; Hamel, S.; Swift, D. C.; Eggert, J. H. Nanosecond X-ray diffraction of shock-compressed superionic water ice. Nature, 2019. **569**(7755) 251-255.
10. Hou, M.; He, Y.; Jang, B. G.; Sun, S.; Zhuang, Y.; Deng, L.; Tang, R.; Chen, J.; Ke, F.; Meng, Y. *et al*, Superionic iron oxide–hydroxide in Earth's deep mantle. Nat. Geosci. 2021. **14**(3) 174-178.
11. Huang, P.; Liu, H.; Lv, J.; Li, Q.; Long, C.; Wang, Y.; Chen, C.; Hemley, R. J.; Ma, Y. Stability of H3O at extreme conditions and implications for the magnetic fields of Uranus and Neptune. Proc. Natl. Acad. Sci. 2020. **117**(11) 5638-5643.
12. French, M.; Mattsson, T. R.; Nettelmann, N.; Redmer, R. Equation of state and phase diagram of water at ultrahigh pressures as in planetary interiors. Phys. Rev. B 2009. **79**(5) 054107.
13. Redmer, R.; Mattsson, Thomas R.; Nettelmann, N.; French, M. The phase diagram of water and the magnetic fields of Uranus and Neptune. Icarus, 2011. **211**(1) 798-803.
14. Sun, J.; Clark, B. K.; Torquato, S.; Car, R. The phase diagram of high-pressure superionic ice. Nat. Commun. 2015. **6**(1) 1-8.
15. Cavazzoni, C.; Chiarotti, G. L.; Scandolo, S.; Tosatti, E.; Bernasconi, M.; Parrinello, M. Superionic and metallic states of water and ammonia at giant planet conditions. Science, 1999. **283**(5398) 44-46.
16. Kamaya, N.; Homma, K.; Yamakawa, Y.; Hirayama, M.; Kanno, R.; Yonemura, M.; Kamiyama, T.; Kato, Y.; Hama, S.; Kawamoto, K. *et al*, A lithium superionic conductor. Nat. Mater. 2011. **10**(9) 682-686.

17. Wang, Y.; Richards, W. D.; Ong, S. P.; Miara, L. J.; Kim, J. C.; Mo, Y.; Ceder, G. Design principles for solid-state lithium superionic conductors. Nat. Mater. 2015. **14**(10) 1026-1031.
18. Zhou, L.; Assoud, A.; Zhang, Q.; Wu, X.; Nazar, L. F. New family of argyrodite thioantimonate lithium superionic conductors. J. Am. Chem. Soc. 2019. **141**(48) 19002-19013.
19. Fujimura, K.; Seko, A.; Koyama, Y.; Kuwabara, A.; Kishida, I.; Shitara, K.; Fisher, C. A. J.; Moriwake, H.; Tanaka, I. Accelerated materials design of lithium superionic conductors based on first-principles calculations and machine learning algorithms. Adv. Energy Mater. 2013. **3**(8) 980-985.
20. Muy, S.; Bachman, J. C.; Chang, H.; Giordano, L.; Maglia, F.; Lupart, S.; Lamp, P.; Zeier, W. G.; Yang, S. Lithium conductivity and Meyer-Neldel rule in Li3PO4-Li3VO4-Li4GeO4 lithium superionic conductors. Chem. Mater. 2018. **30**(16) 5573-5582.
21. Liu, X.; Bjørheim, T.S.; Haugsrud, R. Formation and migration of hydride ions in BaTiO3−xHx oxyhydride. Journal of Materials Chemistry A, 2017. **5**(3) 1050-1056.
22. Liu, X.; Bjørheim, T.S.; Haugsrud, R. Formation of defects and their effects on hydride ion transport properties in a series of K2NiF4-type oxyhydrides. J. Mater. Chem. A 2018. **6**(4) 1454-1461.
23. Verbraeken, M. C.; Suard, E.; Irvine, J. T. Structural and electrical properties of calcium and strontium hydrides. Journal of Materials Chemistry, 2009. **19**(18) 2766-2770.
24. Petkowski, J. J.; Bains, W.; Seager, S. On the potential of silicon as a building block for life. Life, 2020. **10**(6) 84.
25. Feng, J.; Grochala, W.; Jaron, T.; Hoffmann, R.; Bergara, A.; Ashcroft, N. W. Structures and potential superconductivity in SiH 4 at high pressure: En route to “metallic hydrogen”. Phys. Rev. Lett. 2006. **96**(1) 017006.
26. Yao, Y. and Klug, D. D. Silane plus molecular hydrogen as a possible pathway to metallic hydrogen. Proc. Natl. Acad. Sci. 2010. **107**(49) 20893-20898.
27. Pickard, C. J. and Needs, R. J. High-pressure phases of silane. Phys. Rev. Lett. 2006. **97**(4) 045504.
28. Lavvas, P.; Koskinen, T.; Yelle, R. V. Electron densities and alkali atoms in exoplanet atmospheres. Astrophys. J. 2014. **796**(1) 15.
29. Visscher, C.; Lodders, K.; Fegley, B. J. Atmospheric chemistry in giant planets, brown dwarfs, and low-mass dwarf stars. III. Iron, magnesium, and silicon. Astrophys. J. 2010. **716**(2) 1060.
30. Yurchenko, S. N.; Sinden, F.; Lodi, L.; Hill, C.; Gorman, M. N.; Tennyson, J. ExoMol line lists XXIV: A new hot line list for silicon monohydride, SiH. Mon. Not. R. Astron. Soc. 2018. **473**(4) 5324-5333.
31. Noury, S.; Silvi, B.; Gillespie, R. J. Chemical bonding in hypervalent molecules: is the octet rule relevant? Inorg. Chem. 2002. **41**(8) 2164-2172.
32. Puhakainen, K.; Benson, D.; Nylen, J.; Konar, S.; Stoyanov, E.; Leinenweber, K.; Haussermann, U. Hypervalent Octahedral SiH62- Species from High-Pressure Synthesis. Angew. Chem. 2012. **124**(13) 3210-3214.
33. Liang, T.; Zhang, Z.; Feng, X.; Jia, H.; Pickard, C. J.; Redfern, S. A. T.; Duan, D. Ternary hypervalent silicon hydrides via lithium at high pressure. Phys. Rev. Materials, 2020. **4**(11) 113607.

34. Zhang, P.; Sun, Y.; Li, X.; Lv, J.; Liu, H. Structure and superconductivity in compressed Li-Si-H compounds: Density functional theory calculations. Phys. Rev. B 2020. **102**(18) 184103.
35. Pickard, C. J. and Needs, R. J. High-pressure phases of silane. Phys. Rev. Lett. 2006. **97**(4) 045504.
36. Pickard, C. J. and Needs, R. J. Ab initio random structure searching. J. Phys.: Condens. Matter 2011. **23**(5) 053201.
37. Segall, M. D.; Lindan, P. J. D.; Probert, M. J.; Pickard, C. J.; Hasnip, P. J.; Clark, S. J.; Payne, M. C. First-principles simulation: ideas, illustrations and the CASTEP code. J. Phys.: Condens. Matter 2002. **14**(11) 2717.
38. Kresse, G. and Furthmüller, J. Efficiency of ab-initio total energy calculations for metals and semiconductors using a plane-wave basis set. Comput. Mater. Sci. 1996. **6**(1) 15-50.
39. Perdew, J. P.; Burke, K.; Ernzerhof, M. Generalized gradient approximation made simple. Phys. Rev. Lett. 1996. **77**(18) 3865.
40. Blöchl, P. E. Projector augmented-wave method. Phys. Rev. B 1994. **50**(24) 17953.
41. Togo, A.; Oba, F.; Tanaka, I. First-principles calculations of the ferroelastic transition between rutile-type and CaCl2-type SiO2 at high pressures. Phys. Rev. B 2008. **78**(13) 134106.
42. Deringer, V. L.; Tchougreeff, A. L.; Dronskowski, R. Crystal orbital Hamilton population (COHP) analysis as projected from plane-wave basis sets. J. Phys. Chem. A 2011. **115**(21) 5461-5466.
43. Bader, R. F. W. Atoms in Molecules. Acc. Chem. Res. 1985. **18** 9-15.
44. Becke, A.D. and Edgecombe, K. E. A simple measure of electron localization in atomic and molecular systems. J. Chem. Phys. 1990. **92**(9) 5397-5403.
45. Gowers, R. J.; Linke, M.; Barnoud, J.; Reddy, T. J. E.; Melo, M. N.; Seyler, S. L.; Domanski, J.; Dotson, D. L.; and Buchoux, S.; Kenney, I. M. *et al*, MDAnalysis: a Python package for the rapid analysis of molecular dynamics simulations. 2019, Los Alamos National Lab.(LANL).
46. Michaud-Agrawal, N.; Denning, E. J.; Woolf, T. B.; Beckstein, O. MDAnalysis: a toolkit for the analysis of molecular dynamics simulations. J. Comput. Chem. 2011. **32**(10) 2319-2327.
47. Wimmer, E.; Wolf, W.; Sticht, J.; Saxe, P.; G., Clint B.; Najafabadi, Reza; Young, George A. Temperature-dependent diffusion coefficients from ab initio computations: Hydrogen, deuterium, and tritium in nickel. Phys. Rev. B 2008. **77**(13) 134305.